# Influence of sintering temperature and pressure on crystallite size and lattice defect structure in nanocrystalline SiC

J. Gubicza
*Department of Materials Physics, Eötvös Loránd University, H-1518 Budapest, Hungary*

S. Nauyoks
*Department of Physics and Astronomy, Texas Christian University, Fort Worth, TX 76129*

L. Balogh
*Department of Materials Physics, Eötvös Loránd University, H-1518 Budapest, Hungary*

J. Labar
*Department of Materials Physics, Eötvös Loránd University, H-1518 Budapest, Hungary;
and Research Institute for Technical Physics and Materials Science, H-1525 Budapest, Hungary*

T.W. Zerda[a]
*Department of Physics and Astronomy, Texas Christian University, Fort Worth, TX 76129*

T. Ungár
*Department of Materials Physics, Eötvös Loránd University, H-1518 Budapest, Hungary*

Microstructure of sintered nanocrystalline SiC is studied by x-ray line profile analysis and transmission electron microscopy. The lattice defect structure and the crystallite size are determined as a function of pressure between 2 and 5.5 GPa for different sintering temperatures in the range from 1400 to 1800 °C. At a constant sintering temperature, the increase of pressure promotes crystallite growth. At 1800 °C when the pressure reaches 8 GPa, the increase of the crystallite size is impeded. The grain growth during sintering is accompanied by a decrease in the population of planar faults and an increase in the density of dislocations. A critical crystallite size above which dislocations are more abundant than planar defects is suggested.

## I. INTRODUCTION

Silicon carbide is frequently used as a functional and structural material at high temperatures. Nanocrystalline SiC (nc-SiC), offers very high strength in structural applications even at high temperatures.[1] For this reason, silicon carbide often serves as a binding phase in composites, for example in diamond composites. Improvements in mechanical properties of SiC resulting from grain size reduction are expected.[2,3] To modify the grain size of bulk SiC sintered from nanopowders, we varied the manufacturing pressure and temperature. It is expected that the microstructure of sintered SiC can be tailored by the proper selection of these two parameters.[4]

The influence of defects on mechanical properties of ceramics has been thoroughly investigated experimentally,[5] but no theoretical model describing the relationship between deformations in the lattice, hardness, and grain size dependence exists. The lattice defect structure in microcrystalline SiC has been studied by microscopic and x-ray diffraction (XRD) methods.[6,7] The appearance of planar faults in SiC has been reported, and the density of these defects were estimated by comparing intensities of different x-ray reflections.[6,8] However, results of that procedure become uncertain when other lattice defects, such as dislocations, are abundant and the microstructure consists of nanograins. Recently, the convolutional multiple whole profile (CMWP) fitting procedure[9] worked out for the determination of crystallite size and dislocation structures has been extended to determine the density of stacking faults and twins concomitantly with the first two microstructure components.[10] The extended convolutional multiple whole profile (eCMWP) fitting procedure was successfully applied to ultrafine grained copper samples processed by different methods.[10]

In the present work, a series of sintered nc-SiC specimens is investigated by x-ray line profile analysis using the eCMWP fitting procedure. The effect of sintering temperature and pressure on the crystallite size as well as on the dislocation and planar fault densities is studied here. In the past, we applied this methodology to analyze

structure and defects in diamond crystals of different histories of pressure and temperature treatments and in the diamond phase of diamond–SiC composites.[11] Additional motivation for the present study is the need to better understand the role of the SiC binding phase in diamond–SiC composites. Silicon carbide is the weaker component, and its structure and properties determine many physical and mechanical properties of the diamond-based composites. It is expected that the results of this study will help better understand the properties of silicon carbide in those composites that are produced under high-pressure and high-temperature conditions.

## II. EXPERIMENTAL MATERIALS AND PROCEDURES

Bulk nanocrystalline SiC specimens were sintered from SiC nanopowder with nominal grain size of 30 nm. The sintering procedure was carried out at temperatures of 1400, 1600, and 1800 °C. At each temperature, specimens were sintered at pressures of 2, 4, and 5.5 GPa. This process gave nine bulk sintered SiC samples, in addition to the initial powder. An additional specimen was produced at 1800 °C and at a very high sintering pressure of 8 GPa. In each case the sintering time was 10 s.

Sintering at 2 GPa was conducted in a piston–cylinder cell, while those at higher pressures—4, 5.5, and 8 GPa—were sintered in a toroid high pressure cell that consisted of two identical anvils with toroidal grooves and a lithographic gasket that matched the contours of the grooves. In each case, silicon carbide powder was placed inside a heater that consisted of a graphite cylinder and two graphite plugs on both ends of the cylinder. The heater was placed inside a piston–cylinder cell or between the anvils that were next pressed together by a hydrostatic press. Pressure and temperature calibrations were run prior to the experiments according to the procedure described in Ref. 11. Precision of temperature measurements was 50 °C, and pressure was stable within 10%.

The phase composition of the specimens was determined by XRD using a Philips X'pert powder diffractometer (Royal Philips Electronics, The Netherlands) with a Cu anode. The microstructures of the specimens were studied by XRD line profile analysis. The x-ray line profiles were measured by a high-resolution diffractometer (Nonius FR 591, Nonius, France) using Cu K$\alpha_1$ radiation. The line profiles were evaluated by the eCMWP fitting procedure described in detail in Ref. 10. In this method, the experimental pattern is fitted by the convolution of the instrumental pattern and the theoretical size and strain line profiles. Because of the nanocrystalline state of the studied samples, the physical broadening of the profiles was much higher than the instrumental broadening; therefore, instrumental correction

was not applied in the evaluation. The theoretical profile functions used in this fitting procedure were calculated on the basis of a model of the microstructure, where the crystallites have spherical shape and log-normal size distribution, and the lattice strains were assumed to be caused by dislocations and planar faults. Since the crystallite size and the lattice defects only determine the line shape, no conclusions were drawn from the absolute or relative peak intensities. The method gives the area-weighted mean crystallite size, $\langle x \rangle_{area}$; the density of dislocations, $\rho$; and the density of planar fault, in this case twins, $\beta$.

Bright-field images of selected samples were obtained using a Philips CM-20 transmission electron microscope (TEM; Royal Philips Electronics, The Netherlands) operating at 200 kV. Images were recorded on Ditabis imaging plates. The TEM samples were mechanically thinned to about 50 μm, then thinned with 10 kV Ar$^+$ ions from both sides until perforation occurred. Damaged layers on both sides were removed with 2 kV Ar$^+$ ions.

## III. RESULTS AND DISCUSSION

The XRD pattern of the nc-SiC specimen sintered at 2 GPa at 1800 °C is shown in Fig. 1(a) in logarithmic intensity scale. The diffractograms corresponding to the other samples have similar qualitative features. The XRD patterns show that besides the SiC main phase the sintered specimens contain graphite with the concentration between 2 to 5 (±0.5) vol%. These are remnants from the graphite heater that were difficult to remove after the sintering. Because the specimens and the heater were compressed together by the anvils, it was very difficult to remove all graphite without also discarding the specimen. The presence of graphite has a negligible effect on the evaluation of x-ray line profiles of SiC since the peaks of graphite do not overlap with the SiC peaks. The graphite peaks were included in the background during the fitting procedure. The XRD pattern shown in Fig. 1(a) is replotted in Fig. 1(b) with logarithmic intensity scale for the 2θ range between 30 and 45°. A shoulder can be observed on the left tail of the 111 SiC peak at about 2θ = 33.6°. Previous experimental results[6,8] showed that this peak appears when planar faults exist in the microstructure. To justify the correspondence between this small peak and the planar faults, we calculated the XRD pattern for SiC assuming that the microstructure contains planar faults. The calculation was carried out for intrinsic and extrinsic stacking faults and twins by the DIFFaX[12] software. The XRD pattern calculated for 10% twins is plotted in Fig. 2 for the 2θ range between 30° and 45°. The small peak at 33.6° is unambiguously related to planar faults. The same peak also appears when intrinsic or extrinsic stacking faults are assumed in the microstructure.
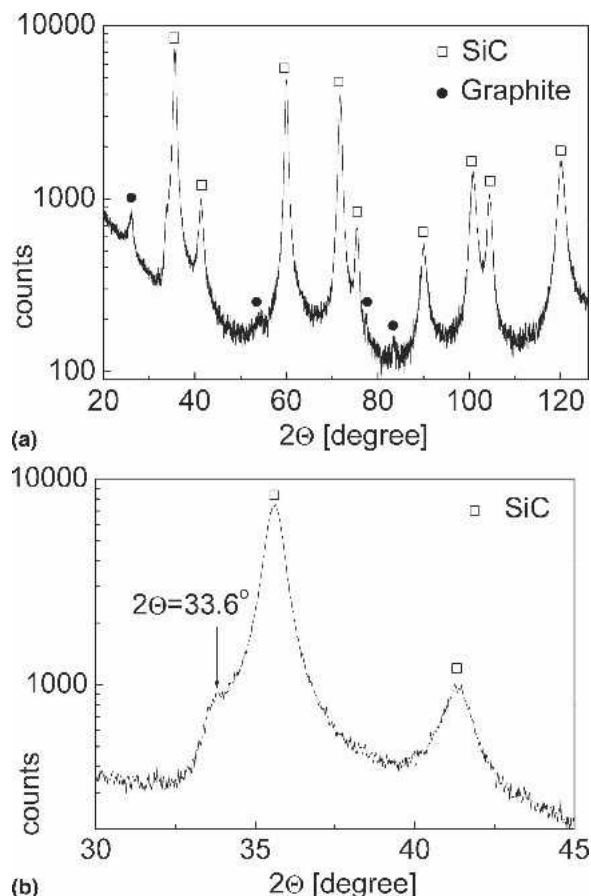
FIG. 1. (a) The x-ray powder diffractogram, in logarithmic scale, for the nc-SiC sample sintered at 2 GPa and 1800 °C and (b) the same pattern for the 2θ range between 30 and 45°.
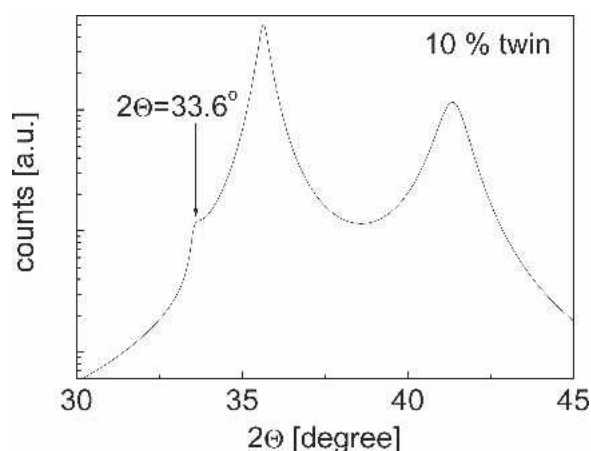


FIG. 2. The calculated x-ray powder diffractogram for nc-SiC containing 10% twins.

For revealing the type of lattice defects in the microstructure, the full width at half-maximum (FWHM) was plotted as a function of the length of the diffraction vector, $K = 2 \sin \theta / \lambda$, in the Williamson–Hall plot. A typical example of the Williamson–Hall plots of the present SiC

samples is shown for the specimen sintered at 2 GPa and 1800 °C in Fig. 3. It can be seen that, within experimental error, the FWHM values of the 111/222 and 200/400 reflection pairs are order-independent, indicating that line broadening, in this case, is mainly caused by small crystallite size and/or planar faults. This is also the case for the initial powder and the specimens sintered at pressures lower than 4 GPa and temperatures below 1600 °C. At the same time, for the nc-SiC specimen sintered at higher pressures and temperatures, e.g., 5.5 GPa and 1800 °C, the breadths of harmonic pairs of reflections are different; i.e., there is a strong order-dependence of the FWHM values, as shown in Fig. 4(a). If the microstructure contains dislocations, the peak breadths have a specific dependence on *hkl* indices.[13] In this case, the FWHM values follow a nonmonotonous line with increasing $K$ in the Williamson–Hall plot; i.e., the breadth of a peak is smaller than that for another peak at a smaller $K$ value.[13] This type of behavior can be observed in Fig. 4(a) for the 400 and 331 reflections. For dislocations, this anisotropic strain broadening is caused by the anisotropic strain field of these lattice defects and the anisotropic elastic constants of the crystal. In the case of dislocations, the strain broadening of a diffraction profile depends on the relative orientations of the line and Burgers vectors of the dislocations and the diffraction vector, similar to the contrast effect of dislocations in electron microscopy. It has been shown that the anisotropic contrast of dislocations in an untextured polycrystalline material can be summarized in the average contrast factors, $C$, which can be calculated numerically on the basis of the crystallography of dislocations and the elastic constants of the crystal.[13] Based on the theory of peak broadening caused by dislocations, it has been shown that in an
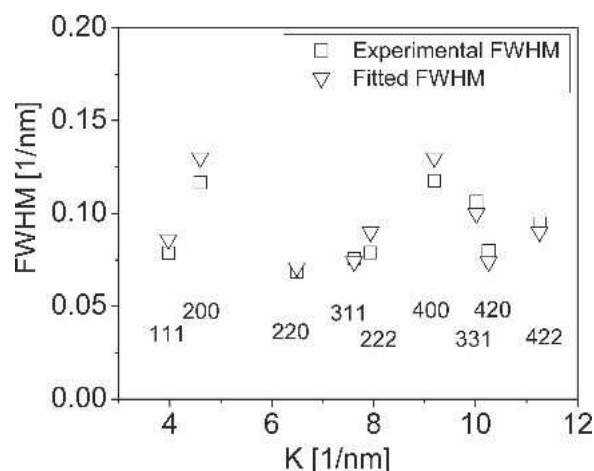


FIG. 3. The Williamson–Hall plot of nc-SiC sintered at 2 GPa and 1800 °C. The squares and the triangles represent the experimentally measured FWHM values and the breadths of the fitting profiles obtained by the convolutional multiple whole profile procedure, respectively.
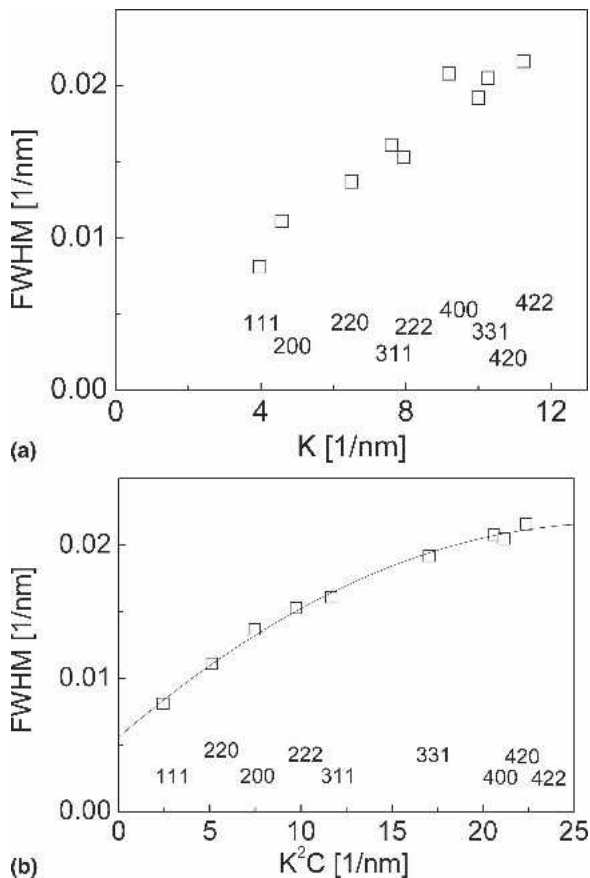
FIG. 4. (a) The conventional Williamson–Hall plot and (b) the modified Williamson–Hall plot for nc-SiC sintered at 5.5 GPa and 1800 °C.

untextured cubic polycrystalline specimen the values of the average $C$ are simple functions of the invariants of the fourth-order polynomials of $hkl$.[13]

$$C = C_{h00}\left(1 - q\frac{h^2k^2 + h^2l^2 + k^2l^2}{(h^2 + k^2 + l^2)^2}\right) \quad , \quad (1)$$

where $C_{h00}$ is the average dislocation contrast factor for the $h00$ reflections and $q$ is a parameter depending on the elastic constants of the crystal and on the character of dislocations (e.g., edge or screw type). Assuming the most common dislocation slip system in SiC with the Burgers vector $\mathbf{b} = a/2 \langle 110\rangle\{111\}$, the values of $q$ for pure screw and pure edge dislocations in silicon carbide are 2.1 and 1.1, respectively. The value of $C_{h00}$ is 0.244 for both types of dislocations. It has been shown that when the anisotropic line broadening is caused by dislocations, the FWHM values depend monotonously on $K^2C$.[12] The plotting of FWHM as a function of $K^2C$ is called the modified Williamson–Hall plot. Figure 4(b) shows the modified Williamson–Hall plot for the reflections of SiC sintered at 5.5 GPa and 1800 °C. Using the value of $q = 1.3$, the FWHM data can be arranged along

a smooth curve in the modified Williamson–Hall plot indicating that lattice distortions originate basically from dislocations. This can be explained by an easier annihilation of screw dislocations at high-temperature deformations of the grains during sintering.

The microstructure parameters of nc-SiC in the initial powder and the sintered specimens were determined by the eCMWP fitting method. For all 11 specimens, the fitting procedure was carried out for extrinsic, intrinsic, and twin planar faults. The final sum of squared residuals after the fitting was the smallest for each sample when twins were assumed. Moreover, for the first two types of planar defects the diffraction lines should show a systematic asymmetry, while in the case of the twins, the peak profiles are expected to be symmetrical.[10] Our profiles were observed to be almost completely symmetrical for all the samples. Taking into account that the smallest values of the final sum of squared residuals were obtained for twins, and that the measured profiles are symmetrical, we conclude that the planar defects are twins. Hereafter, only results obtained by assuming twins as planar faults are shown. Two typical examples of the fitting, one for order-independent and another for order-dependent FWHM behavior are shown in Figs. 5(a) and 5(b) for the samples sintered at 2 and 5.5 GPa at 1800 °C, respectively. The differences between the measured and fitted patterns are also plotted at the bottom of the figures. The quality of the fitting can also be checked in the Williamson–Hall plot of Fig. 3, where the breadths of the fitted profiles (open triangles) are in good agreement with the experimentally determined FWHM values (open squares).

The eCMWP fitting analysis carried out for the initial powder gives the mean crystallite size of 8.3 ± 0.7 nm and the twin density of 7.4 ± 0.6%. As the order-independent FWHM values suggested, the dislocation density (or, in other words microstrain) in the initial powder is below the limit of detection by x-ray line broadening; i.e., $\rho < 10^{13}$ m$^{-2}$. From the results, it can be concluded that in the initial SiC nanopowder the main lattice defects are planar faults, in particular, twin boundaries. Table I shows the microstructure parameters of nine nc-SiC specimens sintered at pressures below 5.5 GPa. The crystallite size increases as a result of sintering. At a constant pressure, the crystallite size increases with temperature and also increases with pressure at a constant temperature. The crystallite size may increase by diffusion of mass from the outer layers of neighboring grains. Statistically equivalent population of threefold and fourfold coordinated atoms has been registered in the outer layers of nanosize SiC grains.[14] The presence of partially disordered structures near the grain boundary has been postulated by Keblinski et al.[15] and detected by Yakamoto et al.[16] and Liao et al.[17] Such structures may facilitate surface diffusion or atom
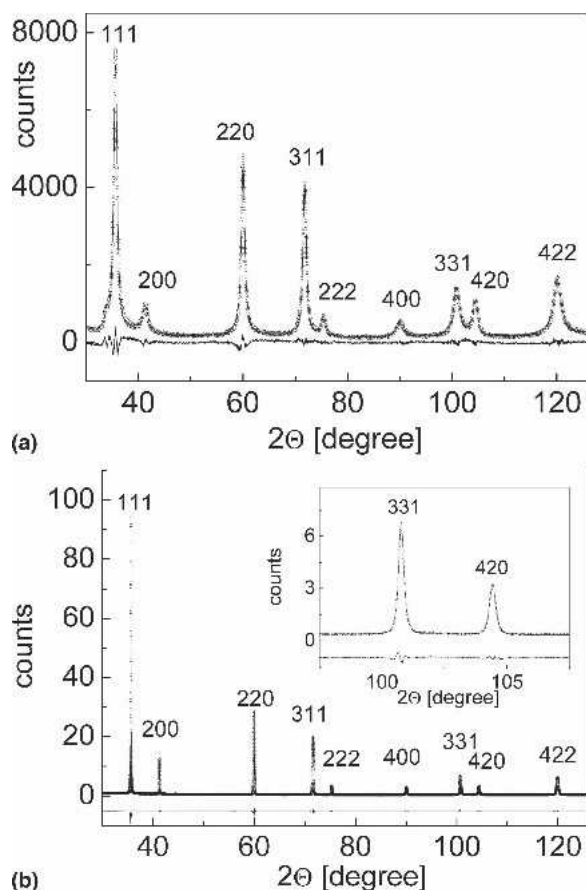
FIG. 5. (a) Convolutional multiple whole profile fitting of the patterns for the sample sintered at 2 GPa and 1800 °C and (b) for the specimen processed at 5.5 GPa and 1800 °C. Open circles and solid line represent the measured and the fitted patterns, respectively.

induce ordering of the amorphous or partially disordered phase leading to larger crystallite sizes.

One can compare the TEM images depicted in Fig. 6 for specimens sintered at 1800 °C and 2, 5.5, and 8 GPa. The values of the grain sizes observed in the TEM images are between 30 and 100 nm, 100 and 300 nm, and 80 and 120 nm for the specimens sintered at 2, 5.5, and 8 GPa, respectively. This trend of the grain size growth with increasing pressure at 1800 °C is consistent with data listed in Table I. The grain sizes obtained by TEM are somewhat larger than the crystallite sizes obtained by x-ray line profile analysis. This difference can be attributed to the fact that x-ray line profile analysis measures the coherently scattering domain size, which is generally smaller than the grain size observable by microscopic methods. The coherency of x-rays scattered from a grain can be broken down by lattice defects, for example, by special arrangement of dislocations. The difference between the grain size determined by TEM and the crystallite size obtained by x-ray line profile analysis has been reported previously; see for example, Ref. 18. This is a general observation for severely deformed materials where dislocations are arranged into low-angle boundaries resulting in small (1 to 2°) misorientations inside the grains, which give only weak contrast difference in TEM images. Moreover, dipolar dislocation walls may also cause the breakdown of coherency of x-ray scattering without misorientations inside a grain; i.e., in this case no contrast difference can be observed in a TEM image taken from that grain.[19] Unfortunately, although the TEM images confirm temperature and pressure dependence of crystallites sizes, they cannot identify the growth mechanism.

At low pressure values, twins are formed during sintering and the dislocation density remains below the detection limit of line profile analysis. At 1600 and 1800 °C, and above a certain pressure limit, the planar fault density decreases to a very low level, i.e., to about $0.1 \pm 0.02\%$, and dislocations become the main type of

rearrangement during the early stages of the sintering process. The increase of temperature causes the increase of mobility of atoms resulting in faster grain growth. Although increased pressure usually reduces mobility of atoms, increased elastic shear strains at the contact surfaces may induce the grain growth. Pressure may also

TABLE I. The parameters of the microstructure for the nc-SiC specimens sintered at different pressures and temperatures.

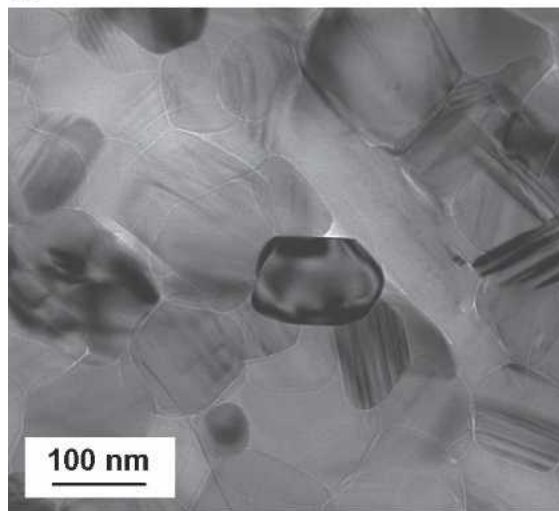| Temperature (°C) | Pressure (GPa) | | |
| --- | --- | --- | --- |
| | 2 | 4 | 5.5 |
| 1400 | $\langle x \rangle_{area} = 8.9 \pm 0.8$ nm $\beta = 9.4 \pm 0.9\%$ $\rho < 10^{13}$ m$^{-2}$ | $\langle x \rangle_{area} = 15 \pm 1$ nm $\beta = 11 \pm 1\%$ $\rho < 10^{13}$ m$^{-2}$ | $\langle x \rangle_{area} = 19 \pm 1$ nm $\beta = 11 \pm 1\%$ $\rho < 10^{13}$ m$^{-2}$ |
| 1600 | $\langle x \rangle_{area} = 13 \pm 1$ nm $\beta = 11 \pm 1\%$ $\rho < 10^{13}$ m$^{-2}$ | $\langle x \rangle_{area} = 16 \pm 1$ nm $\beta = 11 \pm 1\%$ $\rho < 10^{13}$ m$^{-2}$ | $\langle x \rangle_{area} = 94 \pm 7$ nm $\beta = 0.20 \pm 0.03\%$ $\rho = 4.0 \pm 0.8 \times 10^{14}$ m$^{-2}$ |
| 1800 | $\langle x \rangle_{area} = 13 \pm 1$ nm $\beta = 11 \pm 1\%$ $\rho < 10^{13}$ m$^{-2}$ | $\langle x \rangle_{area} = 124 \pm 10$ nm $\beta = 0.10 \pm 0.02\%$ $\rho = 3.0 \pm 0.8 \times 10^{14}$ m$^{-2}$ | $\langle x \rangle_{area} = 126 \pm 10$ nm $\beta = 0.17 \pm 0.03\%$ $\rho = 4.0 \pm 0.8 \times 10^{14}$ m$^{-2}$ |

$\langle x \rangle_{area}$ is the area-weighted mean crystallite size; $\beta$ is the planar fault probability, and $\rho$ is the dislocation density.
The samples containing significant amounts of dislocations are marked by light gray color.
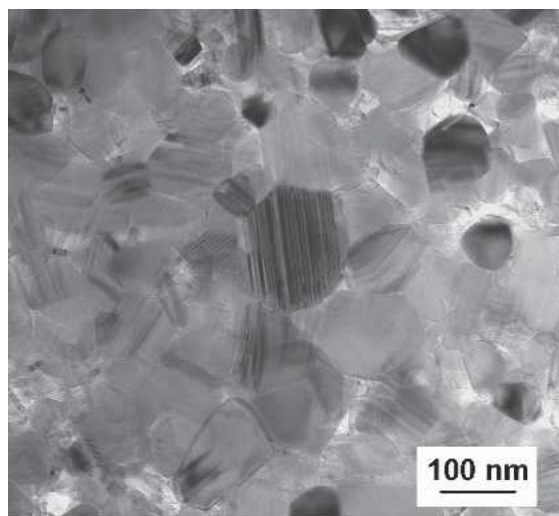
(a)
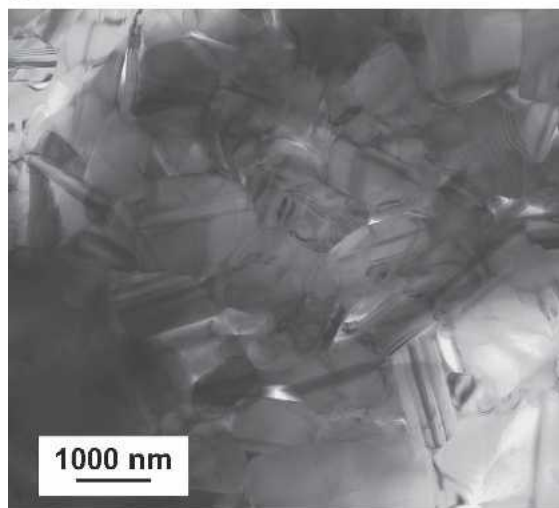


(b)



(c)

FIG. 6. (a) TEM images of specimens sintered at 1800 °C and 2 GPa, (b) 5.5 GPa, and (c) 8 GPa. Please note the different magnification for (b).

lattice defects. This pressure limit decreases with the increase of temperature. The pressure limits are 5.5 and 4 GPa at 1600 and 1800 °C, respectively. It should be noted, however, that for the specimens where dislocations were observed in abundance, the diffraction peak at 33.6° does not completely disappear, indicating small concentration of planar defects in the microstructure. This peak is shown in Fig. 7 in the diffraction pattern for the specimen sintered at 1800 °C and 5.5 GPa. The decrease of the planar fault density when the pressure is increased from 2 to 5.5 GPa at 1800 °C is also justified by the comparison of TEM images in Figs. 6(a) and 6(b). The distances between the planar faults are 3 to 6 nm and 100 to 200 nm for the specimens sintered at 2 and 5.5, respectively. Taking into account that the distance between the neighboring 111 planes in SiC is 0.252 nm, from the TEM images the planar fault density could be evaluated to be in the range 6% to 12% and 0.1% to 0.2%, for the sample prepared at 2 and 5.5 GPa, respectively. These values are close to the planar fault densities determined by x-ray line profile analysis (see Table I). The dislocation density cannot be evaluated from the TEM images.

For the specimen prepared at 8 GPa and 1800 °C the microstructural data are: $\langle x \rangle_{area} = 73 \pm 8$ nm, $\beta = 1.8 \pm 0.3\%$, and $\rho = 15 \pm 2 \times 10^{14}$ m$^{-2}$. The crystallite size decreased while both the dislocation and the planar fault densities increased compared with the sample processed at 5.5 GPa at the same temperature. The TEM images shown in Figs. 6(b) and 6(c) confirm the higher planar fault density and the smaller grain size at 8 GPa compared with the specimen sintered at 5.5 GPa. Although the higher shear strains at 8 GPa could boost the driving force for the increase of the grain size, the diffusion rate and rearrangement of atoms are impeded by increased pressure. The balance between these two mechanisms determines the growth rate. When pressure exceeds a critical value, the grain growth slows down. The average
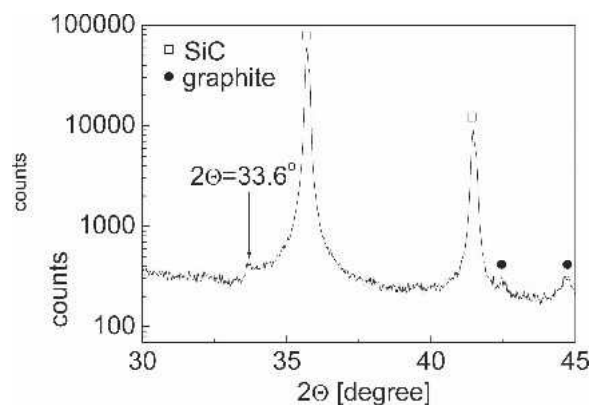


FIG. 7. The x-ray powder diffractogram for nc-SiC sample sintered at 5.5 GPa, 1800 °C in logarithmic intensity scale for the 2θ range between 30 and 45°.

distance between planar faults is 10 to 20 nm for the specimen sintered at 8 GPa. Taking into account that the distance between neighboring 111 planes in SiC is 0.252 nm, from the TEM image for the sample prepared at 8 GPa we estimated the planar fault density as 1% to 2%. This value is close to the planar fault density determined by x-ray line profile analysis; see Table I. The crystallite size, the dislocation density, and the twin density for the 10 sintered specimens as a function of the sintering pressure and temperature are plotted in Figs. 8(a), 8(b), and 8(c), respectively. (The wire grids in the figures are to guide the eye.)

The samples containing a significant amount of dislocations are marked by light gray color in Table I. It seems that at high temperatures and pressures the relatively large crystallite size enables the formation of dislocations during the sintering process. The elimination of planar faults when grain growth takes place during firing at high temperatures has already been observed for SiC.[6] This result is also in line with previous observations for metals.[20] Zhu et al. observed that planar faults are formed in small crystallite sizes, while for crystallites larger than 40 nm dislocations are activated during severe plastic deformation.[20] The value of the crystallite size where that transition takes place depends on the properties of materials. For example, for Cu on the basis of the model calculation and the experimental values of stacking fault energy Zhu and co-workers suggest 40 nm as the critical crystallite size below which deformation proceeds by twinning instead of by dislocation glide.[20] This conclusion was confirmed by Balogh et al.[10] with the use of x-ray line profile analysis. In Fig. 9 the ratio of the twin density and the dislocation density, β/ρ, is shown as a function of the crystallite size for the SiC specimens investigated in this paper. Where the dislocation density was under the detection limit of line profile analysis, the limit was used as the value of the dislocation density. It means that those β/ρ values are probably underestimated; therefore, error bars for the data points are not presented. This, however, does not affect the conclusions drawn from Fig. 9. The figure suggests that with increasing crystallite size the formation of dislocations instead of planar defects is preferred. The current study did not allow us to precisely identify the critical grain size for which dislocations become prevalent, but it is appears to be bounded between 25 and 70 nm.

It has been mentioned previously that the pressure limit, where dislocations become the main lattice defects, decreases with increasing temperature. This phenomenon can be explained by the promoting effect of temperature for the growth of crystallites.[15,16] It is interesting to note that when the crystallite size decreases, e.g., for sintering at 8 GPa and 1800 °C, the planar defects have significant densities, which again supports the observed correlation between the crystallite size and the defect structure.
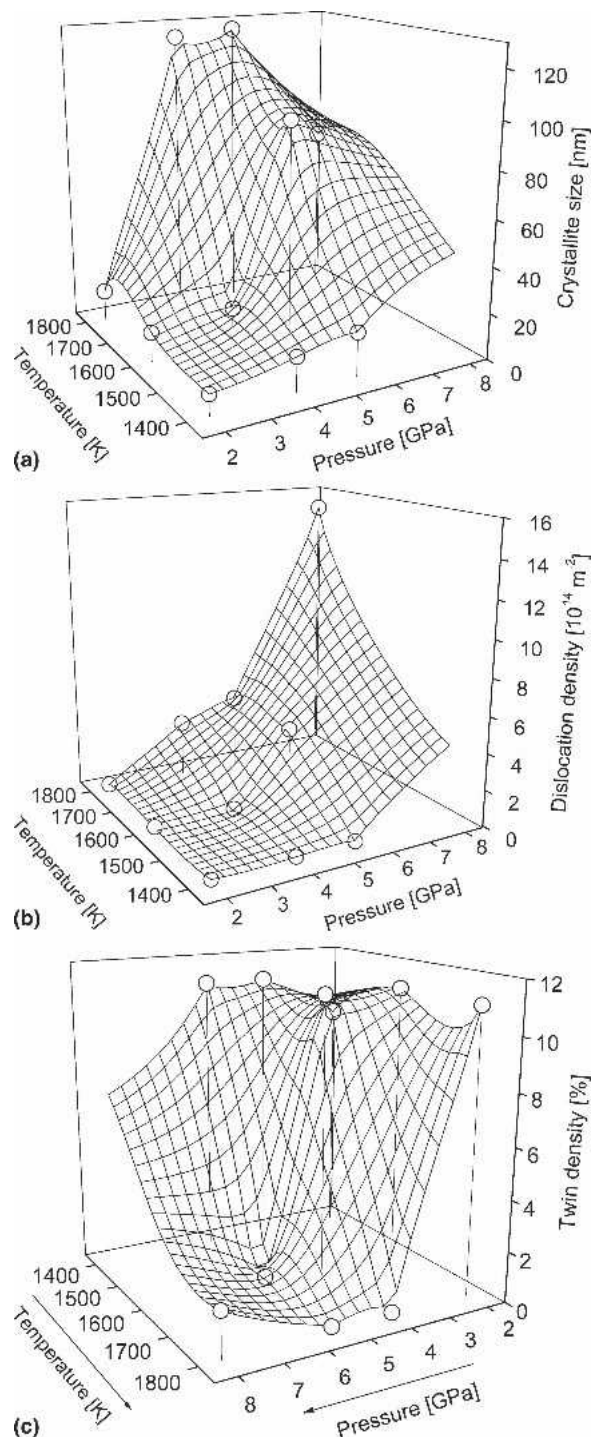


FIG. 8. (a) The crystallite size, (b) the dislocation density, and (c) the twin density for the 10 sintered specimens as a function of the sintering pressure and temperature.

We measured hardness of all specimens; however, since porosity of those samples varied we could not discuss possible correlation between hardness data and factors such as crystallite size, concentration of dislocations, or population of stacking faults.
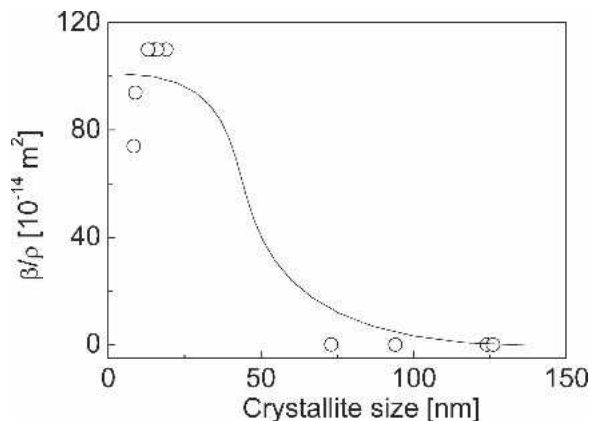
FIG. 9. The ratio of the twin density and the dislocation density ($\beta/\rho$) as a function of the crystallite size for 11 nc-SiC specimens investigated in this paper.

## IV. CONCLUSIONS

The effect of sintering temperature and pressure on the microstructure of bulk nc-SiC manufactured from 30 nm powder was studied by x-ray line profile analysis. This analysis showed that the grain size increases continuously with sintering temperature and pressure, until the pressure reached 8 GPa at 1800 °C. These conditions hampered the grain growth process. Examination of the TEM images confirmed that conclusion. A correlation between the crystallite size and the lattice defect structure was established. The increase of the crystallite size accompanies the reduction of planar fault probability and the increase of the dislocation density. The critical value of crystallite size, where dislocations and not planar faults are the most abundant lattice defects, was estimated to be between 25 and 70 nm.

## REFERENCES

1. Z.H. Huang, D.C. Jia, Y. Zhou, and Y.J. Wang: Effect of a new additive on mechanical properties of hot-pressed silicon carbide ceramics. *Mater. Res. Bull.* **37,** 933 (2002).
2. Y. Zhao, J. Qian, L. Daemen, C. Pantea, J. Zhang, G. Voronin, and T.W. Zerda: Enhancement of fracture toughness in nanostructured diamond–SiC composites. *Appl. Phys. Lett.* **84,** 1356 (2004).
3. I. Szlufarska, A. Nakano, and P. Vashishta: A crossover in the mechanical response of nanocrystalline ceramics. *Science* **309,** 911 (2005).
4. M. Ohyanagi, T. Yamamoto, H. Kitaura, Y. Kodera, T. Ishii, and Z. Munir: Consolidation of nanostructured SiC with disorder-order transformation. *Scripta Mater.* **50,** 111 (2004).
5. A. Krell: *Handbook of Ceramic Hard Materials,* edited by R. Riedel (Wiley-VCH, Weinheim, Germany, 2000), p. 183.
6. K. Koumoto, S. Takeda, C.H. Pai, T. Sato, and H. Yanagida: High-resolution electron microscopy observations of stacking faults in β-SiC. *J. Am. Ceram. Soc.* **72,** 1985 (1989).
7. Y-J. Hao, G-Q. Jin, X-D. Han, and X-Y. Guo: Synthesis and characterization of bamboo-like SiC nanofibers. *Mater. Lett.* **60,** 1334 (2006).
8. H. Tateyama, N. Sutoh, and N. Murukawa: Quantitative analysis of stacking faults in the structure of SiC by x-ray powder profile refinement method. *J. Ceram. Soc. Jpn.* **96,** 1003 (1988).
9. G. Ribárik, J. Gubicza, and T. Ungár: Correlation between strength and microstructure of ball-milled Al–Mg alloys determined by x-ray diffraction. *Mater. Sci. Eng., A* **387–389,** 343 (2004).
10. L. Balogh, G. Ribárik, and T. Ungár: Stacking faults and twin boundaries in fcc crystals determined by x-ray diffraction profile analysis. *J. Appl. Phys.* **100,** 023512 (2006).
11. G.A. Voronin, T.W. Zerda, J. Gubicza, T. Ungar, and S.N. Dub: Properties of nanostructured diamond-silicon carbide composites sintered by high pressure infiltration technique. *J. Mater. Res.* **19,** 2703 (2004).
12. M.M.J. Treacy, J.M. Newsam, and M.W. Deem: A general recursion method for calculating diffracted intensities from crystals containing planar faults. *Proc. R. Soc. London A* **433,** 499 (1991).
13. T. Ungár and G. Tichy: The effect of dislocation contrast on x-ray line profiles in untextured polycrystals. *Phys. Status Solidi A* **147,** 425 (1999).
14. A. Chatterjee, R.K. Kalia, A. Nakano, A. Omeltchenko, K. Tsuruta, P. Vashishta, C.K. Loong, M. Winterer, and S. Klein: Sintering, structure, and mechanical properties of nanophase SiC: A molecular dynamics and neutron scattering study. *Appl. Phys. Lett.* **77,** 1132 (2000).
15. P. Keblinski, D. Wolf, S.R. Phillpot, and H. Gleiter: Continuous thermodynamic-equilibrium glass transition in high-energy grain boundaries. *Philos. Mag. Lett.* **76,** 143 (1997).
16. T. Yamamoto, H. Kitaura, Y. Kodera, T. Ishii, M. Ohyanagi, and Z.A. Munir: Consolidation of nanostructured β-SiC by spark plasma sintering. *J. Am. Ceram. Soc.* **87,** 1436 (2004).
17. F. Liao, S.L. Girshick, W.M. Mook, W.W. Gerberich, and M.R. Zachariah: Superhard nanocrystalline silicon carbide films, *Appl. Phys. Lett.* **86,** 171913 (2005).
18. Y.T. Zhu, J.Y. Huang, J. Gubicza, T. Ungár, Y.M. Wang, E. Ma, and R.Z. Valiev: Nanostructures in Ti processed by severe plastic deformation. *J. Mater. Res.* **18,** 1908 (2003).
19. T. Ungár, G. Tichy, J. Gubicza, and R.J. Hellmig: Correlation between subgrains and coherently-scattering-domains. *J. Powder Diffraction* **20,** 366 (2005).
20. Y.T. Zhu, X.Z. Liao, S.G. Srinivasan, and E.J. Lavernia: Nucleation of deformation twins in nanocrystalline face-centered-cubic metals processed by severe plastic deformation. *J. Appl. Phys.* **98,** 034319 (2005).